

Sensitized photon avalanche nanothermometry in Pr^{3+} and Yb^{3+} co-doped NaYF_4 colloidal nanoparticles

Zuzanna Korczak¹, Magdalena Dudek¹, Martyna Majak¹, Małgorzata Misiak¹,
 Łukasz Marciniak¹, Marcin Szalkowski^{1,2}, and Artur Bednarkiewicz¹

¹*Institute of Low Temperature and Structure Research, Polish Academy of Sciences, 50-422 Wrocław, Poland*

²*Institute of Physics, Faculty of Physics, Astronomy and Informatics, Nicolaus Copernicus University in Toruń
 87-100 Toruń, Poland*

E-mail: A.Bednarkiewicz@intibs.pl

Received November 20, 2022, published online January 25, 2023

Photon avalanche (PA) is a highly nonlinear luminescence phenomenon that occurs in lanthanide doped materials. PA exhibits a very steep power law relationship between luminescence intensity and the optical pump power. Due to the mechanism of PA emission, even weak perturbations to the energy looping and energy distribution within excited levels of lanthanide emitters are expected to significantly modify luminescent properties. Therefore, in this work, we experimentally study the impact of temperature (from -175 to 175 °C, with 25 °C steps) on the sensitized PA emission in NaYF_4 nanoparticles co-doped with 15% of Yb^{3+} and 0.5% of Pr^{3+} ions under 852 nm pumping wavelength. Significant variations of the PA nonlinearity ($S = 4.5\text{--}9$), PA gain (from 50 up to 175), and PA threshold (from 100 up to 700 kW/cm²) were observed under temperature rise from -175 to 175 °C, respectively. The relative temperature sensitivities based on luminescence intensity changes were larger than 1.5% °C⁻¹ in the whole temperature range, reaching the maximal value of 7.5% °C⁻¹ at 0 °C. Moreover, a new thermometric parameter was proposed, namely, the PA pump power threshold, which exhibited over 0.5% °C⁻¹ relative sensitivities in the same wide temperature range. Owing to PA properties, the temperature sensitivity range and the corresponding relative sensitivities may be intentionally tuned by selecting the appropriate pump intensity in respect to the power dependence relationship. These studies not only provide a better understanding of fundamental processes and susceptibility of the sensitized photon avalanche emission to temperature variation, but also show the possibility of using PA materials as sensitive (nano)thermometers.

Keywords: lanthanide doped materials, nanocrystals, luminescence, photon avalanche emission.

1. Introduction

Photon avalanche (PA) is one of the upconversion processes, in which the emitting photon has a higher energy than the excitation photon [1, 2]. There are several conditions that must be met for the PA phenomenon to occur. First, the energy of the excitation photons must resonantly match the transition from the excited state and should mismatch the absorption from the ground state. Typically, the ratio of excited state absorption (ESA) cross-section to ground state absorption (GSA) cross-section, $\sigma_{\text{ESA}}/\sigma_{\text{GSA}}$ should be larger than 10^4 . Moreover, the intermediate level (from which ESA occurs), initially empty, should be efficiently populated in the course of energy looping, which occurs through the mechanisms known as energy cross-relaxation (CR). In conventional phosphors, CR is considered as a parasitic process that depopulates emitting levels

and leads to the so-called concentration quenching, but here, CR is responsible for energy looping between two neighbor ions and enhancement of the population of the intermediate level. Therefore, the PA occurs above a certain critical optical pump power density of the excitation laser (PA threshold) and uniquely shows a highly nonlinear, power law based relationship between pumping power and luminescence intensity (PA slopes), as well as a high (over 100) PA gain.

The PA emission was first observed in infrared quantum counters, LaCl_3 and LaBr_3 doped with Pr^{3+} ions [3]. Since then, the PA phenomenon was also observed in various hosts (bulk crystals, glasses, micro- and aggregated nanoscale materials) singly doped with lanthanide ions (Ho^{3+} , Nd^{3+} , Tm^{3+} , etc.), mainly at low temperatures [2–4]. Sensitized PA (SPA) emission was also demonstrated in Pr^{3+} and Yb^{3+} co-doped

systems, where Yb^{3+} ions play the role of supportive ions (sensitizer like) and are essential for the formation of an energy migration network transferring energy to Pr^{3+} ions [5, 6]. Recently, SPA in nanocrystalline colloidal nanoparticles has been successfully demonstrated and further extended with core-shell energy migration concept to observe multicolor PA emission [7, 8]. In the previous studies, BaY_2F_8 [6], LiYF_4 [5, 9], and NaYF_4 [7] crystals doubly doped with Pr^{3+} and Yb^{3+} ions were excited with wavelength at around 850 nm, which is resonant with ESA from $^1\text{G}_4$ in Pr^{3+} ions and far from resonance for both, Yb^{3+} and Pr^{3+} ions GSA [energy diagram of Pr^{3+} , Yb^{3+} co-doped system was presented schematically in the Fig. 2(a)]. However, even weak absorption from the Yb^{3+} ground state enhances the population of $^1\text{G}_4$ level of Pr^{3+} ions, from which ESA can occur. The latter process and appropriately arranged energy levels in Pr^{3+} ions enable efficient energy looping and the occurrence of PA emission above the pump power threshold. While this system seems to be well understood, only very limited information is known on the susceptibility of PA or SPA emission to temperature in the nanoscale materials [10], which is of great interest for luminescence nanothermometry field and applications [11–13]. Although a single-band ratiometric (SBR) approach strategy was recently proposed [14, 15], which gains from the PA like (i.e., non-GSA) excitation scheme and increased cross-relaxation, all current SBR thermometry studies relied on the sideband ESA and no clear evidences of photon avalanche behavior have been shown so far [14, 16].

In this work, we evaluate the temperature dependent sensitized photon avalanche in NaYF_4 core-passive shell nanocrystals co-doped with 15% of Yb^{3+} and 0.5% of Pr^{3+} ions. Unlike in those previous SBR thermometry studies, we clearly demonstrate all the characteristic features of the PA emission, such as the distinct pump power threshold, the high nonlinearity order of the upconversion emission (S up to 9) and the high PA gains (over 100). The PA emission was recorded at 607 nm ($^3\text{P}_0 \rightarrow ^3\text{H}_6$ transition) and at 482 nm ($^3\text{P}_0 \rightarrow ^3\text{H}_4$ transition) under 852 nm laser excitation. The novelty and major motivation behind our work was to study the above-mentioned relationships in a wide temperature range from -175 up to 175 °C, aiming to understand how the temperature dependent (multi)phonon and cross-relaxation assisted processes affect the sensitized photon avalanche emission at nanoscale.

2. Materials and methods

2.1. Synthesis methods

Reagents. All reagents were used without any further purification. Yttrium oxide Y_2O_3 (99.99%), ytterbium oxide Yb_2O_3 (99.99%), praseodymium oxide Pr_6O_{11} (99.99%) and trifluoroacetic acid (99%) were purchased from Alfa Aesar. Sodium hydroxide NaOH ($\geq 98.0\%$), methanol (99.8%), ethanol (96%), n-hexane (czda), chloroform (98.5%), and

acetic acid (99.5%) were purchased from POCH S.A. Ammonium fluoride NH_4F ($\geq 98.0\%$), octadecene (90%), oleic acid (90%), sodium trifluoroacetate (98%) were purchased from Sigma-Aldrich.

Synthesis of core $\beta\text{-NaYF}_4$: 0.5% Pr^{3+} , 15% Yb^{3+} nanocrystals. The core nanoparticles were prepared by thermal decomposition of oleate salts in high boiling solvents [17]. Initially, a precursor in a form of acetates was prepared. Appropriate amounts of Pr_6O_{11} , Y_2O_3 , and Yb_2O_3 oxides (total amount of 2.5 mmol) were mixed with an acetic acid and water in a 1:1 volume to volume ratio. As prepared mixture was maintained at 200 °C for 2 h in a Teflon-lined autoclave. Afterwards, the solvents were evaporated using a rotary evaporator and dried at 140 °C on a hot plate for one night. Then, 30 ml of oleic acid and 75 ml of 1-octadecene were added to the flask with precursor. The solution was maintained at 140 °C for half an hour under a vacuum to form oleate salts from acetates. Then, the mixture was kept under a nitrogen atmosphere and the temperature was decreased to around 70 °C. Next, a solution of 12 mmol of NaOH and 20 mmol of NH_4F in 13 ml of methanol was added. The mixture was stirred for 10 min at 60 °C. Subsequently, the solution was heated up to 100 °C and left under nitrogen flow for 45 min to slowly evaporate the methanol. Then the temperature was increased to 110 °C and kept under vacuum for 15 min. After the evaporation of methanol, the temperature of the solution was increased to 300 °C and kept for one hour. Subsequently, the solution was cooled to around 80 °C and ethanol was added to precipitate the nanoparticles. Nanoparticles were centrifuged at 10 000 rpm for 10 min. The prepared nanocrystals were washed with n-hexane and again precipitated using ethanol, centrifuged at 14 000 rpm for 10 min and dispersed in 10 ml of chloroform.

Spherical undoped shell deposition. Nanoparticles with spherical shell were synthesized by thermal decomposition of the trifluoroacetates method. First, a precursor was prepared by dissolving of 2.5 mmol of Y_2O_3 in a solution of 10 ml of water and 10 ml of trifluoroacetic acid at 90 °C for 1 h. After cooling to room temperature, solvents were evaporated using a rotary evaporator. The precursor was dried at 140 °C for one night. Subsequently, 5 mmol of sodium trifluoroacetate, 40 ml of oleic acid, and 40 ml of 1-octadecene were added to the round-bottomed flask containing precursor. As prepared solution was kept under a vacuum at 120 °C for half an hour to remove residual oxygen and water. Then the solution was cooled down to 70 °C under a nitrogen atmosphere. 5 ml of colloidal core nanocrystals were added to the flask and the mixture was stirred for 10 min. Then, the temperature was increased to 80 °C and flask was opened for 30 min to evaporate chloroform. Subsequently, the temperature was increased to 110 °C and the solution was kept under vacuum for 15 min to evaporate residual chloroform. Thereafter, under a nitrogen atmosphere, the solution was heated up to 300 °C and kept for 1 h.

After synthesis, the solution was cooled down to around 70 °C and nanoparticles were precipitated using ethanol and centrifuged at 10 000 rpm for 10 min. The nanocrystals were washed with n-hexane and again precipitated with ethanol and centrifuged at 14 000 rpm for 10 min. As prepared nanoparticles were dispersed in 5 ml of chloroform and drop casted on a glass 0.17 mm plate.

2.2. Optical setup

A special optical setup was built to study PA photoluminescence and risetimes in a wide range of excitation power densities (10^2 – 10^7 W cm $^{-2}$). Single mode laser diode (FPL852S — 852 nm, 350 mW, butterfly laser diode, SM Fiber, FC/APC) was used to generate an 852 nm excitation beam. The laser beam passed through the set of neutral density filters, attenuating the excitation light and providing the way for precise control of the power density of the excitation beam. Then the excited beam was reflected by a dichroic mirror (DMSP805R) to the side port of an inverted microscope (Nikon Ti-2 Eclipse). Subsequently, the laser beam is focused by long distance ($f = 20$ mm) objective lens (M Plan Apo 20x) on the sample placed on a microscope slide and kept on heating stage THMS 600 (Linkam), used for temperature control. The intensity of the emission light of the sample (482 nm and 607 nm) was then collected by the same objective lens and, after passing through the dichroic mirror, was recorded by two photomultiplier tube (PMT) detectors (1001M and 2101M, Thorlabs) connected to a photon counter (quTAG, quTOOLS). The emission light was spectrally separated between these two

detecting modules using a DMSP505R dichroic mirror (Thorlabs), and then by F01-475 (Semrock) or 600BP40 (Omega Filters) bandpass filters. With an alternative detection path, emission spectra were registered using an Andor Shamrock i500 spectrograph equipped with a Newton CCD camera (DU920P-BEX2-DD). While the absolute emission intensities measured with the spectrometer and the PMTs are not directly comparable due to differences in spectral sensitivities and transmission of dichroic filters, their relative changes are valid.

2.3. Data analysis

Temperature and pump power dependent luminescence intensity at two spectral bands were analyzed with Origin Lab software, as well as with custom Matlab algorithm, that we have previously developed for analyzing PA properties, with capability to automatically derive PA nonlinearities, PA gain and PA threshold [18].

3. Results and discussion

Based on studies by Y. Liang *et al.* [7], we have synthesized 0.5% Pr^{3+} and 15% Yb^{3+} ions co-doped core and core-shell NaYF $_4$ colloidal nanoparticles. Both, core and core-shell nanoparticles with narrow size distribution [Fig. 1(b)] were characterized by transmission electron microscopy (TEM) [Figs. 1(c)–1(f)]. X-ray diffraction (XRD) confirmed the structural purity of synthesized nanocrystals Fig. 1(a), and the energy dispersive X-ray spectroscopy (EDS) cross-section profile [Fig. 1(h)] evidenced successful passivation of the core nanoparticles with an undoped shell.

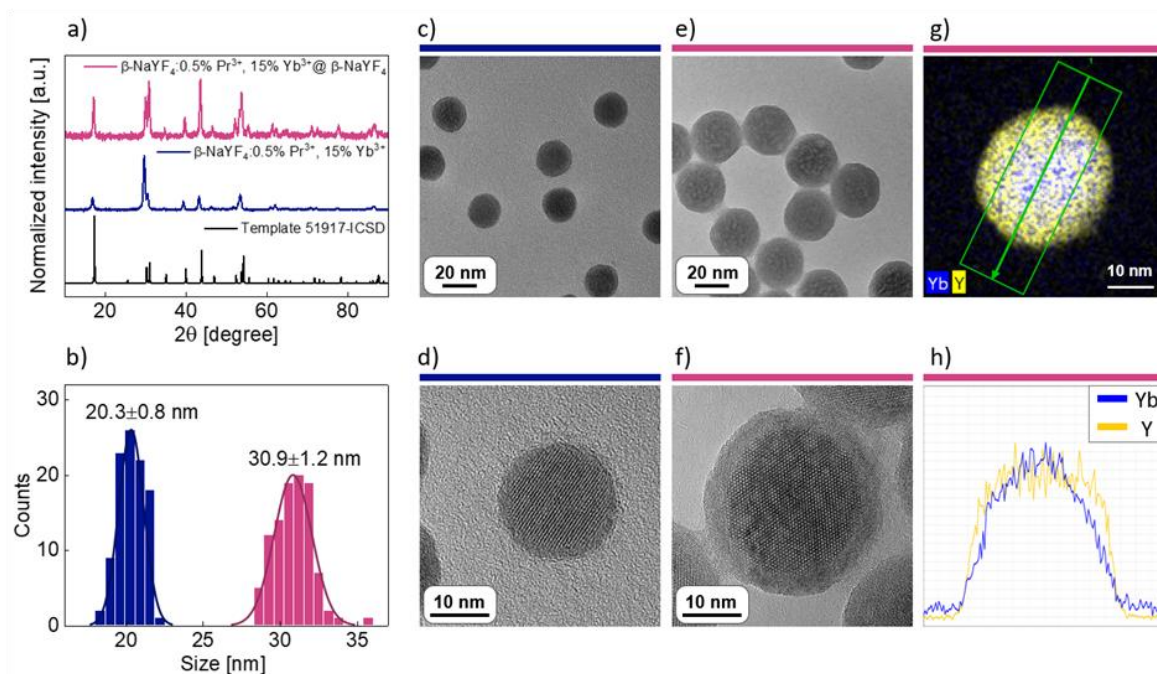


Fig. 1. (Color online) Characterization of core and core-shell nanocrystals co-doped with 0.5% Pr^{3+} and 15% Yb^{3+} ions. (a) X-ray powder diffraction patterns, (b) histograms of nanoparticles; TEM images of (c) core and (e) core-shell nanocrystals; high-resolution transmission electron microscopy (HRTEM) images of (d) core and (f) core-shell nanocrystals; (g) EDS elemental mapping and (h) EDS line scan profiles of Yb^{3+} and Y^{3+} ions in a representative core-shell nanocrystal.

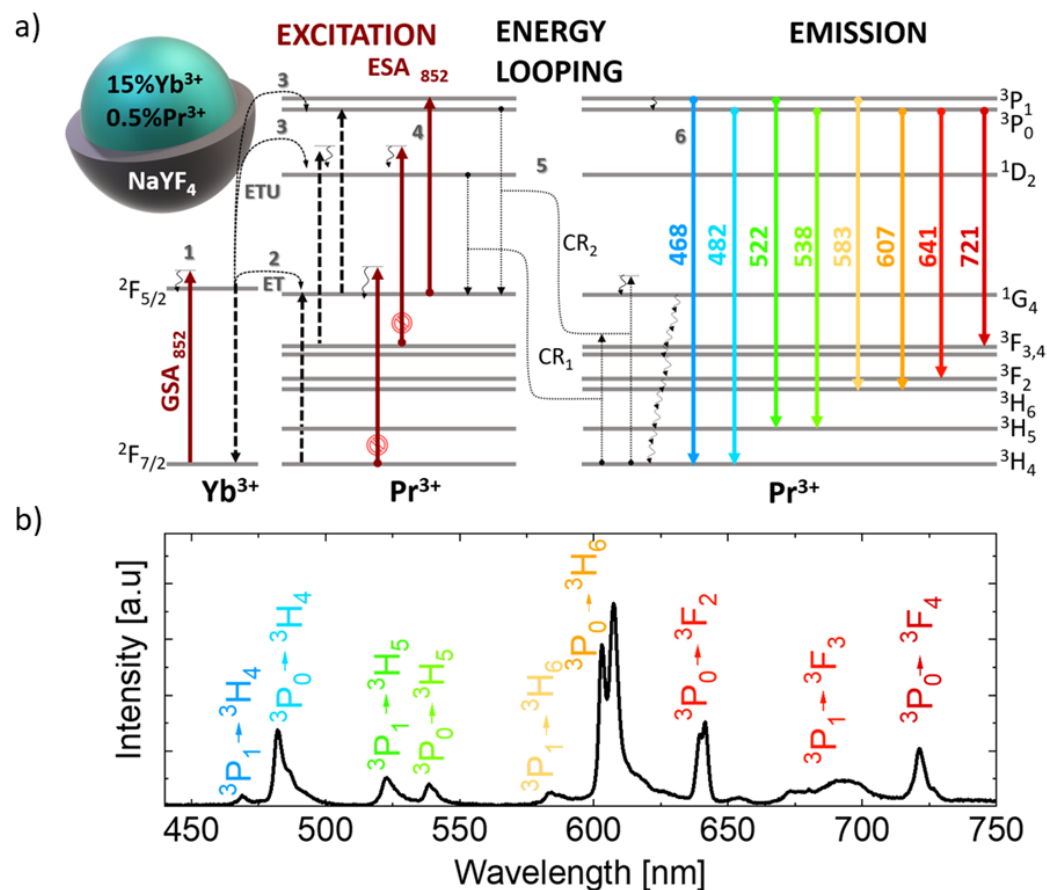


Fig. 2. (Color online) The mechanism and spectral properties of photon avalanching NaYF_4 : 15% Yb^{3+} 0.5% Pr^{3+} @ NaYF_4 nanoparticles. (a) Energy diagram and PA mechanism in Yb^{3+} - Pr^{3+} PA system. (b) Representative photon avalanche emission spectrum of NaYF_4 : 15% Yb^{3+} 0.5% Pr^{3+} @ NaYF_4 under 852 nm excitation (1.5 MW/cm^2) at room temperature. Solid and dotted lines indicate radiative and nonradiative transitions. Wavy arrows indicate multiphonon relaxation processes or phonon assisted energy transfer processes.

The core-shell nanoparticles were characterized spectroscopically for various pump powers in a wide temperature range.

Due to rich structure of the energy levels [Fig. 2(a)], praseodymium ion exhibits many emission bands in the visible range [Fig. 2(b)], such as $3P_1 \rightarrow 3H_4$ (at 468 nm), $3P_0 \rightarrow 3H_4$ (482 nm); $3P_1 \rightarrow 3H_5$ (522 nm); $3P_0 \rightarrow 3H_5$ (538 nm); $3P_1 \rightarrow 3H_6$ (583 nm); $3P_0 \rightarrow 3H_6$ (607 nm); $3P_0 \rightarrow 3F_2$ (641 nm); $3P_0 \rightarrow 3F_{3,4}$ (721 nm). There is an ambiguity in assignment of the ca. 580–620 nm bands to the emission from $3P_1$ or $1D_2$ level across literature reports on various materials and in particular on fluorides [5, 7, 19–24]. For the reasons given below, we accede to the opinion there is no $1D_2$ emission observable in fluorides, and the 583 and 607 nm emission bands originate from the $3P_1 \rightarrow 3H_6$ and $3P_0 \rightarrow 3H_6$ transitions. The spectrum was recorded under 852 nm excitation. This wavelength matches perfectly excited state absorption of Pr^{3+} ions ($1G_4 \rightarrow 3P_1$), but remains off-resonance to ground state absorption, both in Yb^{3+} ions ($2F_{7/2} \rightarrow 2F_{5/2}$, $\Delta E = 1533 \text{ cm}^{-1}$) and Pr^{3+} ions ($3H_4 \rightarrow 1G_4$, $\Delta E = 1887 \text{ cm}^{-1}$) [Fig. 2(a)]. These energy mismatches are however small enough to enable weak side band, phonon assisted absorption that leads to the initial population

of key levels of Yb^{3+} ($2F_{7/2} \rightarrow 2F_{5/2}$) [process (1)] and then of the Pr^{3+} ions (i.e., $1G_4$) as a result of $\text{Yb}^{3+} \rightarrow \text{Pr}^{3+}$ energy transfer (ET) [$\text{Yb}^{3+}:2F_{5/2} \rightarrow \text{Pr}^{3+}:1G_4$, process (2)] and energy transfer upconversion (ETU) [$\text{Yb}^{3+}:2F_{5/2} \rightarrow \text{Pr}^{3+}:1D_2$ or $3P_{0,1}$, processes (3)]. Then, energy looping, provided by cross-relaxation occurs and populates the excited state $1G_4$ [process (5)], what is of crucial importance for PA. Pr^{3+} ions are known to be highly susceptible to concentration quenching even at low concentrations of the activators due to presence of a few possible CR mechanisms between their energy levels, which on the other hand are also powering the energy looping that is essential for PA process. For example, the CR_2 ($3P_0; 3H_4 \rightarrow 1G_4; 1G_4 \pm 950 \text{ cm}^{-1}$) doubles the population of $1G_4$ level, and thus supports ESA excitation, energy looping and ultimately enhances PA behavior. However, the CR_1 ($1D_2; 3H_4 \rightarrow 1G_4; 3F_{3,4} \pm 150 \text{ cm}^{-1}$) quenches the population of $1D_2$ level (if it exists), but it does not contribute to PA gain as it does not double the population of $1G_4$ level (i.e., $3F_{3,4}$ is fed instead), and in consequence it may result in emission quenching by multiphonon relaxation (MPR) to the ground state. The ratio of CR_1 to CR_2 should change with temperature, because the CR_1 requires first $3P_0 \rightarrow 1D_2$ ($\Delta E \approx 3850 \text{ cm}^{-1}$) multiphonon

relaxation to take place, which however is 15.4, 12.6, and 10.5-fold the energy of the phonons available in the NaYF_4 matrix, i.e., 250, 305, and 365 cm^{-1} , respectively. Based on fundamental [25–28], and more recent [10] studies on MPR, we have estimated the MPR rates to stay below 320 s^{-1} for the cut-off 365 cm^{-1} phonons at room temperature. In consequence, this CR_1 process is very unlikely unless ETU from Yb^{3+} occurs, but since no $^1\text{D}_2$ emission is recorded, we suppose the CR_1 is not efficient in the studied system. Therefore, the only possible CR that may play a role here is the CR_2 (energy mismatch equals $\Delta E \approx 950 \text{ cm}^{-1}$) process, which requires 3 phonons of 305 cm^{-1} energy and thus should be highly probable. Because all MPR are phonon (defined by host matrix) and temperature dependent [10], lower temperatures should further diminish the $^3\text{P}_0 \rightarrow ^1\text{D}_2$ MPR and thus should support “beneficial” CR_2 ($\Delta E \approx 150 \text{ cm}^{-1}$) over “parasitic” CR_1 ($\Delta E \approx 950 \text{ cm}^{-1}$). To understand the actual role of temperature in PA emission, the intensities of the two most intense emission bands ($^3\text{P}_0 \rightarrow ^3\text{H}_4$ at 482 nm and $^3\text{P}_0 \rightarrow ^3\text{H}_6$ at 607 nm) were measured for temperature rising from -175 to 175 $^\circ\text{C}$ with 25 $^\circ\text{C}$ steps [Fig. 3]. Both profiles are very similar, the luminescence lifetimes at these wavelengths are identical and equal to *ca.* 19 μs at room temperature. This is quite obvious as the two emission bands originate from the same $^3\text{P}_0$ level.

The luminescence pump power dependence studies [Figs. 3(a) and 3(e), at 607 and 482 nm, respectively] clearly demonstrate typical photon avalanche behavior in

the whole studied temperature range. Above a distinct pump power threshold [Figs. 3(a)–3(d) and 3(e)–3(h)], the intensity of the luminescence increases steeply [Figs. 3(a), 3(b) and 3(e), 3(f)] and then saturates with a further increase of pump power. The slope of the curves [Figs. 3(b) and 3(f)] measured for different temperatures varied between *ca.* 6 and 9.3, but in most cases values from 7 to 8 were obtained. The photon avalanche gain (D_{av}), defined as the increase in luminescence intensity (I_{lum}) when the intensity of the excitation beam (I_{exc}) is doubled [18], is expressed as

$$D_{\text{av}}(I_{\text{exc}}) = \frac{I_{\text{lum}}(2 \cdot I_{\text{exc}})}{I_{\text{lum}}(I_{\text{exc}})}. \quad (1)$$

The highest D_{av} [Figs. 3(c) and 3(g)] reached 179.6 at 482 nm emission at 25 $^\circ\text{C}$. These pump power dependent profiles, high values of S_{max} and D_{av} , as well as a distinct pump power PA threshold clearly confirm the photon avalanche character of the observed emission. Moreover, temperature studies indicate the significant influence of temperature on PA phenomenon. The decrease of temperature from 175 $^\circ\text{C}$ down to -175 $^\circ\text{C}$ enhances PA emission intensity by 2–3 orders of magnitude [Figs. 3(a) and 3(e)], decreases the nonlinearity up to 2-fold [Figs. 3(b) and 3(f)] and lowers PA gain *ca.* 3–4-fold [Figs. 3(c) and 3(g)]. Concurrently, PA threshold becomes 10-fold lower [Figs. 3(d) and 3(h)]. At low temperature, the luminescence behavior resembles energy looping rather than photon avalanche

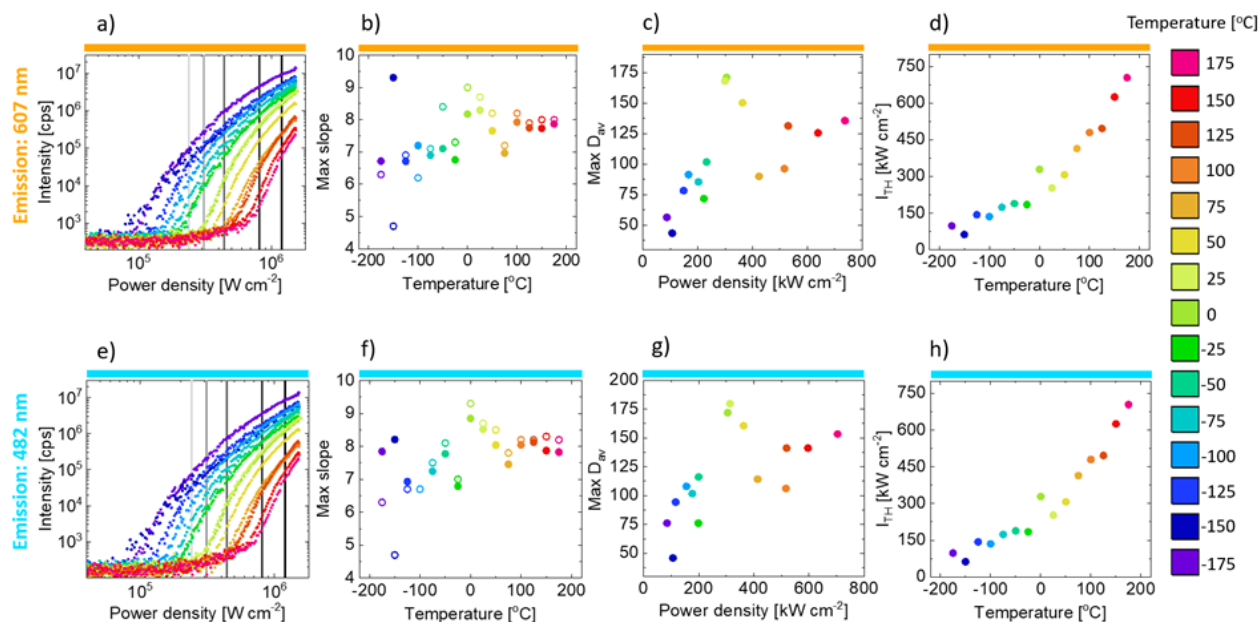


Fig. 3. (Color online) Temperature and pump power characterization of the photon avalanche emission in NaYF_4 : 15% Yb^{3+} 0.5% Pr^{3+} @ NaYF_4 under 852 nm excitation. Top and bottom rows correspond to orange 607 nm and blue 482 nm emission bands, respectively. (a) and (e) show pump power dependence of photon avalanche emission intensity for various temperatures. (b) and (f) show the highest PA nonlinearities S_{max} derived manually (open circles) and by the algorithm described in Ref. 18 (full circles); (c) and (g) demonstrate maximal PA gain at the excitation intensity corresponding to the highest nonlinearity [i.e., $D_{\text{av}}(I_{\text{exc}} @ S_{\text{max}})$], (d) and (h) show PA threshold at various temperatures. (b)–(h) datasets were derived from the pump power dependencies (a) and (e) at various temperatures.

(lower slopes and gains), while at higher temperature the emission power dependence shows more photon avalanche behavior (i.e., higher slopes). These evidences indicate a complex nature of the sensitized PA phenomenon in Yb^{3+} , Pr^{3+} co-doped NaYF_4 nanoparticles. On the one hand, lowering temperature reduces multiphonon-relaxation, non-radiative quenching on the surface or internal losses, which is evidenced by lower pump power PA threshold. While surface quenching is reduced by surface passivation, the losses include efficient cross-relaxations between Pr^{3+} ions and fast MPR between the levels below $10\,000\text{ cm}^{-1}$ ($^1\text{G}_4 \rightarrow ^3\text{F}_{3,4} \rightarrow ^3\text{F}_2 \rightarrow ^3\text{H}_6 \rightarrow ^3\text{H}_5 \rightarrow ^3\text{H}_4$). On the other hand, the energy gap mismatches between energy levels of Yb^{3+} and Pr^{3+} ions require phonon assistance, therefore lower temperature obviously hinders energy looping between the two ions. This is somehow contradictory to expectations, as CR_2 starts to dominate over possible CR_1 , and this trend should enhance PA performance. But one should be aware of the complicated sequence of processes that lead to sensitized PA emission. These include strongly temperature dependent absorption of Yb^{3+} in fluoride matrix [29], which affect not only process (1) in Fig. 2(a), but also energy transfer between Yb^{3+} and Pr^{3+} [processes (2) and (3) in Fig. 2(a)]. Moreover, more CR processes can be expected in rich energy level scheme of Pr^{3+} ions than the most probable CR_2 (and hypothetical CR_1) presented in Fig. 2(a). These CRs may further hinder understanding of the temperature dependent phenomena studied here. Lowering temperature leads to (a) *ca.* 100-fold enhanced luminescence intensity, (b) lowering PA nonlinearities, (c) lowering PA gains, and (d) lowering PA threshold. The first and last effects are

obviously resulting from reduced MPR quenching of intermediate and emitting levels of Pr^{3+} activators, which are expected to disrupt energy looping. However, lower PA slopes [Figs. 3(b) and 3(f)] and PA gains [Figs. 3(c) and 3(g)] should indicate that the CR_2 is affected by temperature to a larger extent than the CR_1 . Firstly, one should keep in mind that CR_2 is critical to achieve PA emission in Pr^{3+} ions, while CR_1 should be considered as parasitic one. Secondly, one should also understand the energy mismatch in $\Delta E(\text{CR}_2)$ is larger (and thus more temperature and host matrix dependent) than $\Delta E(\text{CR}_1)$, therefore the CR_2 energy looping should be more temperature dependent. In consequence, we should conclude, the PA emission in sensitized Pr^{3+} ions results from a complex balance between a set of direct (ESA) and sensitized ($\text{Yb}^{3+} \rightarrow \text{Pr}^{3+}$) photoexcitation, phonon assisted energy looping and MPR quenching mechanisms.

To further evaluate the temperature responsiveness of the studied sensitized PA system, PA emission intensity versus rising temperatures was studied for a few, arbitrarily selected pump power densities (vertical gray lines marked in Figs. 3(a) and 3(e), at 0.24, 0.31, 0.44, 0.81, and $1.20\text{ MW}\cdot\text{cm}^{-2}$). These data points were extracted from original datasets [Figs. 3(a) and 3(e)] and further used in the subsequent analysis in Fig. 4. Approximately, with increasing temperature, the luminescence intensity decreases exponentially. The temperature change led to PA intensity increase by over 2–3 orders of magnitude. At the same time, due to the highly nonlinear behavior of PA emission, the PA intensity is highly susceptible to small instabilities of the excitation laser power, mechanical drift of the optical set-up, and other experimental factors. For these reasons,

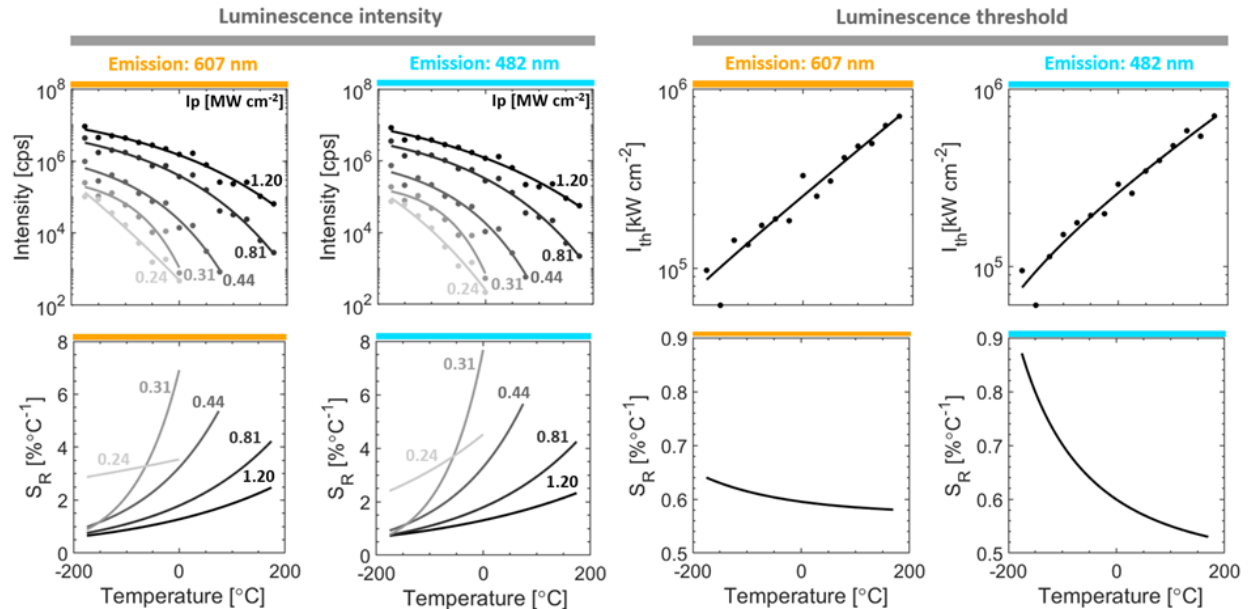


Fig. 4. (Color online) Temperature dependence of photon avalanche luminescence of NaYF_4 : 15% Yb^{3+} 0.5% Pr^{3+} under 852 nm photo-excitation. Temperature dependence of PA luminescence intensity, $I_{\text{lum}}(T)$, at (a) 607 nm and (c) 482 nm for selected pump power intensities ($I_p = 0.24, 0.31, 0.44, 0.81$, and $1.20\text{ MW}\cdot\text{cm}^{-2}$); (b) and (d) show corresponding relative temperature sensitivities. Temperature dependence of PA threshold, $I_{\text{th}}(T)$, for emission at (e) 607 nm and (g) 482 nm. (f) and (h) show corresponding relative temperature sensitivities. The data presented here are based on experimental data presented in Figs. 3(a) and 3(e).

the experimental PA intensities were neither perfectly smooth nor monotonic. Therefore, to enable quantitative evaluation of temperature dependence, the experimental data points were first fit with an exponential curve, from which the relative sensitivity (S_R) could be counted by the well-known formula [30]:

$$S_R = \frac{1}{\theta} \frac{\Delta\theta}{\Delta T} 100\%, \quad (2)$$

where θ is a thermometric parameter, e.g., this can be either luminescence intensity ($\theta = I_{\text{lum}}$), luminescence intensity ratio ($\theta = \text{LIR}$) or PA pump power threshold ($\theta = I_{\text{th}}$), the $\Delta\theta$ indicates luminescence thermometric parameter change corresponding to ΔT temperature change.

Depending on the choice of excitation power, one can intentionally choose greater S_R at the expense of the operating range of such a thermometer. If a wide operating range of the thermometer is preferred, a lower S_R is obtained or the opposite. The highest S_R of $7.5\% \text{ } ^\circ\text{C}^{-1}$ was obtained for emission at 482 nm under excitation power density of $0.31 \text{ MW}\cdot\text{cm}^{-2}$ for temperatures below $0 \text{ } ^\circ\text{C}$. Similar properties (S_R of $7.0\% \text{ } ^\circ\text{C}^{-1}$) were found for 607 nm emission in the same conditions. These sensitivities significantly exceed those reported for ESA ($1.29\% \text{ } ^\circ\text{C}^{-1}$ for $\text{KLaP}_4\text{O}_{12}:\text{Pr}^{3+}$ [31] and $5\% \text{ } ^\circ\text{C}^{-1}$ for $\text{LaF}_3:\text{Pr}^{3+}$ [24]) where true PA phenomenon was not observed despite using ESA based excitation scheme.

In addition, based on the exponential temperature dependence of the PA threshold (I_{th}) as a new thermometric parameter, relative sensitivities were calculated to be up to $0.9\% \text{ } ^\circ\text{C}^{-1}$ for 482 nm emission at low temperature. The relative sensitivities were no less than $0.5\% \text{ } ^\circ\text{C}^{-1}$ at both emission wavelengths in the whole temperature range from -175 up to $175 \text{ } ^\circ\text{C}$.

The very high relative sensitivity values, predicted previously theoretically for avalanching systems [10], could be used for ultraprecise luminescence nanothermometry. The proposed single emission band intensity approach, despite it offers a rather straightforward relationship between the intensity and temperature, simplify the experimental setup and data interpretation, is immanently connected with several limitations in real life applications, which should be underlined. Firstly, when the avalanching temperature nanoprobe is surrounded by the scattering or absorbing environment (i.e., sample volume), the luminescence intensity based temperature measurement is affected in two ways. First of all, part of the emitted light is attenuated, especially from the visible range, far from transmission window of biological tissues, like in the presented $\text{Pr}^{3+}\text{Yb}^{3+}$ based system. However, a much more significant influence of scattering medium, even when limited by using NIR excitation light, comes from attenuating of the pump light. This is due to the very nonlinear relation between the excitation power and resulting luminescence intensity characterizing avalanching materials. In such case, even minute decrease in the excitation power density

translates to steep decrease in the emission intensity, thus leading to incorrect temperature measurement. In addition, the inhomogeneous distribution of nanoparticles in the system significantly affects the luminescence intensity readout and thus the temperature measurement. A similar problem was described for thermometers based on the other excited state absorption processes. In that case, in order to eliminate the aforementioned limitations of the reliability of the temperature reading based on the intensity of a single band, a single-band ratiometric approach strategy was proposed and discussed in detail previously [10, 15, 16]. Additional GSA pumped probe reference signal that is less sensitive to the influence of the attenuating medium and temperature variation can be used in real-life applications.

The ratiometric approaches (SBR or LIR) are widely used and feasible, but these methods are not always reliable enough in terms of flexibility, optimum temperature operating range and often require relatively complicated and expensive detection instrumentation, which may hinder wider adoption of luminescence based nanothermometry in technology and biomedical sciences. Therefore, not only more sensitive, brighter and robust phosphors are sought, but also novel temperature sensing schemes, which may potentially simplify remote quantification and imaging of temperature. Hence, PA-based thermometers, due to their high relative sensitivities and monotonic behavior, reveal promising thermometric performance despite the fact that the lack of information on what power density reaches the sample still remains a significant limitation.

Beside consideration on the suitability of the studied materials for thermometry, the data presented in Fig. 4 confirms previous discussion about a complex nature of photon avalanche emission in Pr^{3+} , Yb^{3+} SPA system. Namely, various temperature and pump power dependent processes contribute to energy excitation and absorption, energy transfer and distribution, as well as energy looping and emission. A qualitative explanation of the observed relationships must be followed by developing and solving an appropriate numerical model of the sensitized PA emission like in Ref. 10 to further advance understanding and enable optimization of the Pr^{3+} , Yb^{3+} photon avalanche luminescence.

Conclusions

We reported the temperature dependent PA behavior in the colloidal core-shell NaYF_4 : 15% Yb^{3+} 0.5% Pr^{3+} nanocrystals. In this system, energy looping, responsible for powering PA emission, occurs between the ESA-pumped Pr^{3+} ions, but is also supported by the presence of the Yb^{3+} sensitizer ions. The PA phenomenon, with significant temperature dependence of the emission intensity and the PA threshold, was clearly observed in the entire studied temperature range (from -175 to $175 \text{ } ^\circ\text{C}$). A completely novel thermometric approach for luminescence thermometry, based on the use of threshold excitation power to observe PA

luminescence (I_{th}) as a thermometric parameter was proposed. A gradual shift of the PA threshold towards higher excitation power densities (from 100 to 750 kW·cm⁻²) was observed with increasing temperature. This approach assured relative temperature sensitivity above 0.5% °C⁻¹. Simultaneously, with increasing temperature the emission intensity at 482 and 607 nm decreases significantly up to four orders of magnitude for selected excitation powers. Based on such substantial changes in the intensity of a single emission band the corresponding temperature relative sensitivity was calculated and the maximum value of 7.5% °C⁻¹ was obtained at 0 °C. These relationships not only confirm suitability of such approach for luminescence thermometry, but also evidence a complex set of coexisting phenomena that drive PA emission. The presented results demonstrate, that the PA emission in sensitized Pr³⁺ ions results from a complex balance between a set of direct (ESA) and sensitized (Yb³⁺ → Pr³⁺) photoexcitation, phonon assisted (therefore temperature dependent) energy looping and MPR quenching mechanisms.

Acknowledgments

The authors acknowledge financial support from projects 2018/31/B/ST5/01827 and 2021/43/B//01244 funded by the National Science Center, Poland. The calculations were performed using resources provided by the Wrocław Network and Supercomputing Center (<http://wcsc.pl>), Grant No. 529.

1. F. Auzel, *Upconversion and anti-stokes processes with f and d ions in solids*, *Chem. Rev.* **104**, 139 (2004).
2. M. F. Joubert, S. Guy, B. Jacquier, and C. Linarés, *The photon-avalanche effect: review, model and application*, *Opt. Mater. (Amst)* **4**, 43 (1994).
3. J. S. Chivian, W. E. Case, and D. D. Eden, *The photon avalanche: A new phenomenon in Pr³⁺-based infrared quantum counters*, *Appl. Phys. Lett.* **35**, 124 (1979).
4. M.-F. Joubert, S. Guy, B. Jacquier, and C. Linarés, *Opt. Mater.* **4**, 43 (1994).
5. S. Küick, A. Dening, E. Heumann, et al., *Avalanche up-conversion processes in Pr, Yb-doped materials*, *J. Alloys Compd.* **300**, 65 (2000).
6. E. Osiac, A. Dening, E. Heumann, et al., *Spectroscopic characterisation of the upconversion avalanche mechanism in Pr³⁺, Yb³⁺:BaY₂F₈*, *Opt. Mater. (Amst)* **24**, 537 (2003).
7. Yusen Liang, Zhimin Zhu, Shuqian Qiao, et al., *Migrating photon avalanche in different emitters at the nanoscale enables 46th-order optical nonlinearity*, *Nat. Nanotechnol.* **17**, 524 (2022).
8. A. Bednarkiewicz and M. Szalkowski, *Photon avalanche goes multicolour*, *Nat. Nanotechnol.* **17**, 440 (2022).
9. S. Küick and I. Sokólska, *The up-conversion of near-infrared excitation radiation in Ho³⁺-doped LiYF₄*, *Chem. Phys. Lett.* **325**, 257 (2000).
10. M. Szalkowski, M. Dudek, Z. Korczak, et al., *Predicting the impact of temperature dependent multi-phonon relaxation processes on the photon avalanche behavior in Tm³⁺: NaYF₄ nanoparticles*, *Opt. Mater.: X* **12**, 100102 (2021).
11. Miroslav Dramicanin, *Luminescence Thermometry: Methods, Materials and Applications*. Woodhead Publishing, Elsevier (2018).
12. C. D. S. Brites, A. Millán, and L. D. D. Carlos, *Lanthanides in Luminescent Thermometry, Handbook on the Physics and Chemistry of Rare Earth* **49**, 339 (2016).
13. A. Bednarkiewicz, J. Drabik, K. Trejgis, D. Jaque, E. Ximendes, and L. Marciniak, *Luminescence based temperature bio-imaging: Status, challenges, and perspectives*, *Appl. Phys. Rev.* **8**, 011317 (2021).
14. L. Marciniak, A. Bednarkiewicz, and K. Elzbieciak, *NIR-NIR photon avalanche based luminescent thermometry with Nd³⁺-doped nanoparticles*, *J. Mater. Chem. C* **6**, 7568 (2018).
15. A. Bednarkiewicz, K. Trejgis, J. Drabik, A. Kowalczyk, and L. Marciniak, *Phosphor-assisted temperature sensing and imaging using resonant and nonresonant photoexcitation scheme*, *ACS Appl. Mater. Interfaces* **9**, 43081 (2017).
16. K. Trejgis, A. Bednarkiewicz, and Ł. Marciniak, *Engineering excited state absorption based nanothermometry for temperature sensing and imaging*, *Nanoscale* **12**, 4667 (2020).
17. K. A. Abel, J. C. Boyer, and F. C. J. M. van Veggel, *Hard proof of the NaYF₄/NaGdF₄ nanocrystal core/shell structure*, *J. Am. Chem. Soc.* **131**, 14644 (2009).
18. M. Dudek, M. Szalkowski, M. Misiak, et al., *Size-dependent photon avalanching in Tm³⁺-doped LiYF₄ nano, micro, and bulk crystals*, *Adv. Opt. Mater.* **10**, 2201052 (2022).
19. P. Boutinaud, R. Mahiou, N. Martin, and M. Malinowski, *Luminescence from Pr³⁺3P₁ and ³P₂ states in β-NaYF₄: Pr³⁺*, *J. Lumin.* **72–74**, 809 (1997).
20. S. Hao, W. Shao, H. Qiu, et al., *Tuning the size and upconversion emission of NaYF₄:Yb³⁺/Pr³⁺ nanoparticles through Yb³⁺ doping*, *RSC Adv.* **4**, 56302 (2014).
21. M. Y. Tsang, P. Fałat, M. A. Antoniuk, et al., *Pr³⁺-doped NaYF₄ and LiYF₄ nanocrystals combining visible-to-UVC upconversion and NIR-to-NIR-II downconversion luminescence emissions for biomedical applications*, *Nanoscale* **14**, 14770 (2022).
22. M.-F. F. Joubert, *Photon avalanche upconversion in rare earth laser materials*, *Opt. Mater. (Amst)* **11**, 181 (1999).
23. T. R. Gosnell, *Avalanche assisted upconversion in Pr³⁺/Yb³⁺-doped ZBLAN glass*, *Electron Lett.* **33**, 411 (1997).
24. J. Stefanska and L. Marciniak, *Single-band ratiometric luminescent thermometry using Pr³⁺ ions emitting in yellow and red spectral ranges*, *Adv. Photonics Res.* **2**, 2100070 (2021).
25. M. J. Weber, *Multiphonon relaxation of rare-earth ions in yttrium orthoaluminate*, *Phys. Rev. B* **8**, 54 (1973).
26. T. Miyakawa and D. L. Dexter, *Phonon sidebands, multiphonon relaxation of excited states, and phonon-assisted energy transfer between ions in solids*, *Phys. Rev. B* **1**, 2961 (1970).

27. A. Meijerink, G. Blasse, J. Sytsma, C. de Mello Donega, and A. Ellens, *Electron-phonon coupling in rare earth compounds*, *Acta Phys. Pol. A* **90**, 109 (1996).
28. N. Yamada, S. Shionoya, and T. Kushida, *Phonon-assisted energy transfer between trivalent rare earth ions*, *J. Physical Soc Jpn.* **32**, 1577 (1972).
29. D. V. Seletskiy, S. D. Melgaard, R. I. Epstein, A. di Lieto, M. Tonelli, and M. Sheik-Bahae, *Precise determination of minimum achievable temperature for solid-state optical refrigeration*, *J. Lumin.* **133**, 5 (2013).
30. A. Bednarkiewicz, L. Marciniak, L. D. D. Carlos, and D. Jaque, *Standardizing luminescence nanothermometry for biomedical applications*, *Nanoscale* **12**, 14405 (2020).
31. J. Stefanska, K. Maciejewska, and L. Marciniak, *Blue-emitting single band ratiometric luminescent thermometry based on $\text{LaF}_3\text{:Pr}^{3+}$* , *New J. Chem.* **45**, 11898 (2021).

Сенсибілізована фотонна лавинна
нотермометрія в колоїдних наночастинках
 NaYF_4 , легованих Pr^{3+} та Yb^{3+}

Zuzanna Korczak, Magdalena Dudek,
Martyna Majak, Małgorzata Misiak, Łukasz Marciniak,
Marcin Szalkowski, Artur Bednarkiewicz

Фотонна лавина (ФЛ) — це надзвичайно нелінійне явище люмінесценції, яке виникає в матеріалах, легованих лантаноїдами. ФЛ демонструє дуже круту степеневу залежність між інтенсивністю люмінесценції та потужністю оптичної накачки. Завдяки механізму випромінювання ФЛ

навіть слабкі збурення енергетичного циклу та розподілу енергії в межах збуджених рівнів лантаноїдних випромінювачів, як очікується, можуть суттєво змінити люмінесцентні властивості. Експериментально досліджено вплив температури (від -175 до 175 °C, з кроком 25 °C) на випромінювання сенсибілізованої ФЛ у наночастинках NaYF_4 , легованих 15% Yb^{3+} та $0,5\%$ Pr^{3+} , при довжині хвилі накачування 852 нм. Значні зміни нелінійності ФЛ ($S = 4,5\text{--}9$), коефіцієнта підсилення ФЛ (від 50 до 175) та порогу ФЛ (від 100 до 700 кВт/см²) спостерігалися при підвищенні температури від -175 до 175 °C відповідно. Відносна температурна чутливість, яка заснована на змінах інтенсивності люмінесценції, була більшою за $1,5\%$ °C⁻¹ у всьому діапазоні температур, досягаючи максимального значення $7,5\%$ °C⁻¹ при 0 °C. Крім того, запропоновано новий термометричний параметр, а саме: поріг потужності накачування ФЛ, який демонстрував відносну чутливість понад $0,5\%$ °C⁻¹ у тому ж широкому діапазоні температур. Завдяки властивостям ФЛ діапазон температурної чутливості та відповідна відносна чутливість можуть бути цілеспрямовано налаштовані шляхом вибору відповідної інтенсивності накачки з урахуванням залежності від потужності. Проведені дослідження не тільки забезпечують краще розуміння фундаментальних процесів чутливості сенсибілізованої фотонної лавинної емісії до зміни температури, але також показують можливість використання ФЛ матеріалів як чутливих (нано)термометрів.

Ключові слова: матеріали, що доповані лантаноїдами, нанокристали, люмінесценція, лавинне випромінювання фотонів.